

# Quasi-elastic neutrino charged-current scattering off $^{12}\text{C}$ : effects of the meson exchange currents and large nucleon axial mass

A. V. Butkevich<sup>1</sup> and S. V. Luchuk<sup>1,2</sup>

<sup>1</sup>*Institute for Nuclear Research, Russian Academy of Sciences, Moscow 117312, Russia*

<sup>2</sup>*Moscow Institute of Physics and Technology, Dolgoprudny 141701, Russia*

(Dated: November 5, 2018)

The quasi-elastic scattering of muon neutrino and electrons on a carbon target are analyzed using the relativistic distorted-wave impulse approximation (RDWIA). We also evaluate the contribution of the two-particle and two-hole meson exchange current ( $2p - 2h$  MEC) to electroweak response functions. The nuclear model dependence of the (anti)neutrino cross sections is studied within the RDWIA+MEC approach and RDWIA model with the large nucleon axial mass. It is shown that the results for the squared momentum transfer distribution  $d\sigma/dQ^2$  and for invariant mass of the final hadronic system distribution  $d\sigma/dW$  obtained within these models are substantially different.

PACS numbers: 25.30.-c, 25.30.Bf, 25.30.Pt, 13.15.+g

## I. INTRODUCTION

One of the important goals of the current [1, 2] and upcoming [3, 4] accelerator-based neutrino experiments is the determination of the neutrino masses ordering. The question is whether we have two “light” and one “heavy” neutrino (the so-called normal mass hierarchy) or two “heavy” and one “light” neutrino (the inverted hierarchy). When neutrino propagate through a medium the oscillation physics is modified by the so-called matter effect [5, 6]. Matter effects depend on the ordering of the neutrino mass eigenstates and allow one to probe the mass hierarchy in different ways. Thanks to the matter effects in the Sun, we know that  $\nu_1$  is lighter than  $\nu_2$ , where  $(\nu_1, \nu_2, \nu_3)$  are neutrino with well-defined masses. For  $\nu_1(\nu_2)$  and  $\nu_3$  sector, matter effects in the Earth’s crust are significant (about 30%) for neutrino energy  $\varepsilon_\nu \sim 1 \div 5$  GeV and propagation distance  $L \sim 10^3$  km.

In this energy regime the dominant contribution to the neutrino-nucleus cross section

comes from the charged-current (CC) quasielastic (CCQE) reactions, two-body meson exchange current (MEC), and resonance production processes. To evaluate the neutrino mass-square difference in muon neutrino oscillation experiments, the probabilities of  $\nu_\mu$  disappearance and  $\nu_e$  appearance versus neutrino energy are measured. At neutrino energy  $\varepsilon_\nu \geq 2$  GeV the contribution of the CCQE scattering is less than 40% and therefore the incoming neutrino energy is estimated applying the calorimetric energy reconstruction method, already actively used in experiments.

Conservation of total energy in CC neutrino interactions implies  $\varepsilon_\nu = \varepsilon_f + \varepsilon_h$ , where  $\varepsilon_f$  and  $\varepsilon_h$  are lepton and hadronic energies, respectively. Thus, the total hadronic energy deposit is the necessary information for calorimetric method. Muon energy is reconstructed from the measured path length in the detector. Hadronic energy is obtained from calorimetry by first summing all the visible energy not associated with the muon. However, it is impossible to measure energies of all hadrons, notable energy deposits by neutrons are always hard to measure. A model dependent fit obtained from simulation is used to relate the summed visible energy to the estimated total hadronic energy. This procedure is not free from systematic uncertainties affecting the determination of the incident neutrino energy. For instance, the estimated muon and hadronic energy resolution are 3.5% and 25%, respectively, giving an overall energy resolution for selected  $\nu_\mu$ -CC events of about 7% for fully active and fine-grained NOvA detectors [7].

In addition to its role in reconstruction of the incident neutrino energy, the hadronic energy plays an essential role in studying CCQE interactions. Note, as the quasielastic interaction is a two-particle scattering process, it forms a CCQE interaction sample and energy of the incoming neutrino can be derived from lepton kinematics alone. The measurement of muon momentum and angle allows one to estimate neutrino energy  $\varepsilon_\nu^{QE}$  and the squared four-momentum transfer  $Q_{QE}^2$ , assuming the target nucleon at rest. This reconstruction method (kinematic method) works well if the true nature of events were indeed a CCQE process. Therefore accuracy of the kinematic neutrino energy reconstruction method depends on the purity of the CCQE sample, and therefore measurements of the differential  $d\sigma/dQ_{QE}^2$  and total  $\sigma(\varepsilon_\nu^{QE})$  cross sections are model dependent. Note, the calorimetric method can also be applied to the CCQE events. Modern neutrino experiments are investigating the axial-vector current contribution to the quasielastic neutrino scattering on nuclei. For estimation of neutrino energy, the kinematic method is applied. Using the dipole parametrization of the

axial form factor and the values of  $\epsilon_{\nu}^{QE}$  and  $Q_{QE}^2$ , these experiments have extracted within the relativistic Fermi gas model (RFGM) [8] the values of  $M_A \approx 1.2 \div 1.4$  GeV, that are systematically higher than  $M_A \approx 1$  GeV obtained from deuterium target.

These results have stimulated many theoretical studies trying to explain the apparent discrepancies between data and theoretical predictions. A detailed review of the experimental results and theoretical framework of neutrino-nucleus CCQE-like interaction can be found elsewhere (see for instance [9, 10] and references therein). Based on the results from different groups [11–18] it is shown that CCQE-like data are really a combination of genuine QE and  $np - nh$  contributions. The inclusion of two-particle and two-hole ( $2p - 2h$ ) meson exchange current (MEC) contributions, has allowed one to explain experimental results without modification of the axial mass, (i.e., with  $M_A \approx 1$  GeV). The MEC effects play an important role in the “dip” region between the QE and  $\Delta$  peaks, where the energy of the hadronic final system produced in the two-body MEC processes is larger than in the CCQE interaction. That is why, there is a growing interest in utilizing hadron information to study MEC contributions. On the other hand, with detector that can directly measure at least a part of the hadronic energy, the  $2p - 2h$  contribution to the CCQE events sample can be reduced. In this case the MEC contributions are treated as background, and one would expect CCQE sample to provide the cross sections that more or less agree with the RFGM predictions with  $M_A \approx 1$  GeV (the so-called golden scenario).

In this work we perform a joint calculation of the CCQE and  $2p - 2h$  contributions to lepton scattering cross sections on carbon, using the relativistic distorted-wave impulse approximation (RDWIA) with  $M_A = 1.03$  GeV for quasielastic responses and the  $2p - 2h$  meson exchange currents response functions in the electroweak sector (RDWIA+MEC prediction). We also calculate (anti)neutrino cross sections within the RDWIA approach with  $M_A = 1.35$  GeV. The RDWIA, which takes into account the nuclear shell structure and final state interaction (FSI) effects, was developed for description of QE electron-nucleus scattering and was successfully tested against the data [19–21]. This approach was also applied to neutrino-nucleus interactions to calculate the genuine QE cross sections [22–27]. In our approach [24, 25] the effects of the short-range nucleon-nucleon ( $NN$ )- correlations in the nuclei ground state are estimated.

To evaluate the MEC response we use simple parameterizations of the exact MEC calculations of the electroweak response as functions of the momentum and energy transfer.

These calculations were performed within RFGM. The functional forms employed for the parameterizations of the transverse electromagnetic vector response, and for axial and vector components of the weak response were detailed in [16, 18]. These parameterizations have been validated by describing the full set data of inclusive cross section of electron scattering on carbon [28] and data from the neutrino experiments [18]. The results show good agreement with experimental data over wide range of energy transfer.

The aim of this work is twofold. First, we test the RDWIA+MEC approach with  $^{12}\text{C}(e, e')$  scattering data for different kinematic situations. The accordance between this model predictions and data in the vector sector gives us confidence in the extension of this phenomenological approach and its validity, when applied to calculation of the CCQE-like cross sections of the (anti)neutrino scattering on carbon. Second, we compare the neutrino cross sections calculated in the RDWIA+MEC and RDWIA (with  $M_A = 1.35$  GeV) approaches to study the effects due to the MEC contributions and large nucleon axial mass. This issue is very important for neutrino oscillation experiments, provided that the two effects (whether one changes the transverse response or axial form factor) have very different consequences on the energy dependence of the CCQE cross section and the determination of  $\varepsilon_\nu$ .

The paper is organized as follows. In Sec. II we briefly introduce the formalism needed for studying quasielastic lepton scattering off nuclei with the  $2p - 2h$  MEC contributions, and describe the RDWIA model and our MEC calculations. The results are presented and discussed in Sec. III. Our conclusions are summarized in Sec. IV.

## II. FORMALISM OF QUASIELASTIC SCATTERING, RDWIA, AND $2p - 2h$ MEC RESPONSES

We consider electron and neutrino charged-current QE inclusive

$$l(k_i) + A(p_A) \rightarrow l'(k_f) + X \quad (1)$$

scattering off nuclei in the one-photon (W-boson) exchange approximation. Here  $l$  labels the incident lepton [electron or muon (anti)neutrino], and  $l'$  represents the scattered lepton (electron or muon),  $k_i = (\varepsilon_i, \mathbf{k}_i)$  and  $k_f = (\varepsilon_f, \mathbf{k}_f)$  are the initial and final lepton momenta,  $p_A = (\varepsilon_A, \mathbf{p}_A)$  is the initial target momenta,  $q = (\omega, \mathbf{q})$  is the momentum transfer carried by the virtual photon (W-boson), and  $Q^2 = -q^2 = \mathbf{q}^2 - \omega^2$  is the photon (W-boson) virtuality.

### A. Quasielastic lepton-nucleus cross sections

In the inclusive reactions (1) only the outgoing lepton is detected and the differential cross sections can be written as

$$\frac{d^3\sigma^{el}}{d\varepsilon_f d\Omega_f} = \frac{\varepsilon_f \alpha^2}{\varepsilon_i Q^4} L_{\mu\nu}^{(el)} W^{\mu\nu(el)}, \quad (2a)$$

$$\frac{d^3\sigma^{cc}}{d\varepsilon_f d\Omega_f} = \frac{1}{(2\pi)^2} \frac{|\mathbf{k}_f|}{\varepsilon_i} \frac{G^2 \cos^2 \theta_c}{2} L_{\mu\nu}^{(cc)} W^{\mu\nu(cc)}, \quad (2b)$$

where  $\Omega_f = (\theta, \phi)$  is the solid angle for the lepton momentum,  $\alpha \simeq 1/137$  is the fine-structure constant,  $G \simeq 1.16639 \times 10^{-11} \text{ MeV}^{-2}$  is the Fermi constant,  $\theta_C$  is the Cabbibo angle ( $\cos \theta_C \approx 0.9749$ ),  $L_{\mu\nu}$  is the lepton tensor,  $W^{\mu\nu(el)}$  and  $W^{\mu\nu(cc)}$  are correspondingly the electromagnetic and weak CC nuclear tensors. In terms of response functions the cross sections reduce to

$$\frac{d^3\sigma^{el}}{d\varepsilon_f d\Omega_f} = \sigma_M (V_L R_L^{(el)} + V_T R_T^{(el)}), \quad (3a)$$

$$\frac{d^3\sigma^{cc}}{d\varepsilon_f d\Omega_f} = \frac{G^2 \cos^2 \theta_c}{(2\pi)^2} \varepsilon_f |\mathbf{k}_f| (v_0 R_0 + v_T R_T + v_{zz} R_{zz} - v_{0z} R_{0z} - h v_{xy} R_{xy}), \quad (3b)$$

where

$$\sigma_M = \frac{\alpha^2 \cos^2 \theta / 2}{4\varepsilon_i^2 \sin^4 \theta / 2} \quad (4)$$

is the Mott cross section. The electron  $V_k$  and neutrino  $v_k$  coupling coefficients, whose expressions are given in [24] are kinematic factors depending on the lepton's kinematics.

The response functions are given in terms of components of the hadronic tensors

$$R_L^{(el)} = W^{00(el)}, \quad (5a)$$

$$R_T^{(el)} = W^{xx(el)} + W^{yy(el)}, \quad (5b)$$

$$R_0 = W^{00(cc)}, \quad (5c)$$

$$R_T = W^{xx(cc)} + W^{yy(cc)}, \quad (5d)$$

$$R_{0z} = W^{0z(cc)} + W^{z0(cc)}, \quad (5e)$$

$$R_{zz} = W^{zz(cc)}, \quad (5f)$$

$$R_{xy} = i (W^{xy(cc)} - W^{yx(cc)}), \quad (5g)$$

and depend on the variables  $(Q^2, \omega)$  or  $(|q|, \omega)$ . They describe the electromagnetic and weak properties of the hadronic system.

All the nuclear structure information and final state interaction effects (FSI) are contained in the electromagnetic or weak CC nuclear tensors. They are given by the bilinear products of the transition matrix elements of the nuclear electromagnetic or CC operator  $J_\mu^{(el)(cc)}$  between the initial nucleus state  $|A\rangle$  and the final state  $|X\rangle$  as

$$W_{\mu\nu} = \sum_f \langle X | J_\mu^{(el)(CC)} | A \rangle \langle A | J_\nu^{(el)(CC)\dagger} | X \rangle, \quad (6)$$

where the sum is taken over undetected states  $X$ . This equation is very general and includes all possible final states. Thus, the hadron tensors can be expanded as the sum of  $1p-1h$  and  $2p-2h$ , plus additional channels:

$$W^{\mu\nu} = W_{1p1h}^{\mu\nu} + W_{2p2h}^{\mu\nu} + \dots \quad (7)$$

In the impulse approximation (IA) the  $1p-1h$  channel gives the well-known CCQE response functions and the  $2p-2h$  hadronic tensor determines the  $2p-2h$  MEC response functions. Thus, the functions  $R_i$  (5) can be written as a sum of the CCQE ( $R_{i,QE}$ ) and MEC ( $R_{i,MEC}$ ) response functions

$$R_i = R_{i,QE} + R_{i,MEC} \quad (8)$$

## B. RDWIA model

We describe genuine CCQE neutrino-nuclear scattering in the impulse approximation (IA), assuming that the incoming neutrino interacts with only one nucleon, which is subsequently emitted, while the remaining (A-1) nucleons in the target are spectators. The nuclear current is written as the sum of single-nucleon currents.

For electron scattering, we use the CC2 electromagnetic vertex function for a free nucleon [29]

$$\Gamma_V^\mu = F_V^{(el)}(Q^2)\gamma^\mu + i\sigma^{\mu\nu}\frac{q_\nu}{2m}F_M^{(el)}(Q^2), \quad (9)$$

where  $\sigma^{\mu\nu} = i[\gamma^\mu, \gamma^\nu]/2$ ,  $F_V^{(el)}$  and  $F_M^{(el)}$  are the Dirac and Pauli nucleon form factors. The single-nucleon charged current has  $V-A$  structure  $J^{\mu(cc)} = J_V^\mu + J_A^\mu$ . For a free-nucleon vertex function  $\Gamma^{\mu(cc)} = \Gamma_V^\mu + \Gamma_A^\mu$  we use the CC2 vector current vertex function

$$\Gamma_V^\mu = F_V(Q^2)\gamma^\mu + i\sigma^{\mu\nu}\frac{q_\nu}{2m}F_M(Q^2) \quad (10)$$

and the axial current vertex function

$$\Gamma_A^\mu = F_A(Q^2)\gamma^\mu\gamma_5 + F_P(Q^2)q^\mu\gamma_5. \quad (11)$$

The weak vector form factors  $F_V$  and  $F_M$  are related to the corresponding electromagnetic form factors  $F_V^{(el)}$  and  $F_M^{(el)}$  for protons and neutrons by the hypothesis of the conserved vector current. We use the approximation of Ref. [30] for the Dirac and Pauli nucleon form factors. Because the bound nucleons are off-shell we employ the de Forest prescription [29] and Coulomb gauge for off-shell vector current vertex  $\Gamma_V^\mu$ . The vector-axial  $F_A$  and pseudoscalar  $F_P$  form factors are parametrized using a dipole approximation:

$$F_A(Q^2) = \frac{F_A(0)}{(1 + Q^2/M_A^2)^2}, \quad F_P(Q^2) = \frac{2mF_A(Q^2)}{m_\pi^2 + Q^2}, \quad (12)$$

where  $F_A(0) = 1.267$ ,  $M_A$  is the axial mass, which controls  $Q^2$ -dependence of  $F_A(Q^2)$ , and  $m_\pi$  is the pion mass.

In the RDWIA, the relativistic wave functions of the bound nucleon states are calculated in the independent particle shell model as the self-consistent solutions of a Dirac equation, derived within a relativistic mean field approach, from a Lagrangian containing  $\sigma, \omega$ , and  $\rho$  mesons (the  $\sigma - \omega$  model)[31, 32]. According to the JLab data [21, 33] the occupancy of the independent particle shell-model orbitals of  $^{12}\text{C}$  equals on average 89%. In this work, we assume that the missing strength (11%) can be attributed to the short-range  $NN$ -correlations in the ground state, leading to the appearance of the high-momentum and high-energy component in the nucleon distribution in the target. These estimates of the depletion of hole states are consistent with a direct measurement of the spectral function [34], which observed approximately 0.6 protons in a region attributable to a single-nucleon knockout from a correlated cluster. In the RDWIA, final state interaction effects for the outgoing nucleon are taken into account. The distorted-wave function of the knocked out nucleon is evaluated as a solution of a Dirac equation containing a phenomenological relativistic optical potential. The LEA program [35] for the numerical calculation of the distorted wave functions with the EDAD1 parametrization [36] of the relativistic optical potential for carbon was used. We calculated the inclusive and total cross sections with the EDAD1 relativistic optical potential in which only the real part was included.

The cross sections with the FSI effects in the presence of the short-range  $NN$ -correlations were calculated by using the method proposed in Ref. [24] with the nucleon high-momentum

distribution from Ref. [37] that was renormalized to value of 11%. In this approach, the contribution of the  $NN$ -correlated pairs is evaluated in impulse approximation, i.e., the virtual photon (W-boson) couples to only one member of the  $NN$ -pair. It is a one-body process that leads to the emission of two nucleons ( $2p - 2h$  excitation).

### C. $2p - 2h$ excitation

In order to evaluate the  $2p - 2h$  hadronic tensor  $W_{2p2h}^{\mu\nu}$ , in Refs. [15, 17] the RFGM was chosen to describe the nuclear ground state. The short-range  $NN$ -correlations and FSI effects were not considered in this approach. The elementary hadronic tensor is given by bilinear product of the matrix elements of the two-body electromagnetic or weak (containing vector and axial components) MEC. Only one-pion exchange is included.

The two-body current operator is obtained from the electroweak pion production amplitudes for the nucleon [38] with coupling a second nucleon to the emitted pion. The pion-production amplitudes are derived in the non-linear  $\sigma$ -model for the  $\gamma(W)N \rightarrow N'\pi$  reaction together with electroweak excitation of the  $\Delta(1232)$  resonance and its subsequent decay into  $\pi N$ . The resulting MEC operator can be written as a sum of seagull, pion-in-flight, pion-pole, and Delta-pole operators. The  $\Delta$ -peak is the main contribution to the pion production cross section. But inside the nucleus  $\Delta$  can also decay into one nucleon that re-scatters producing two-nucleon emission without pions. Therefore, this decay of  $\Delta$  should be considered as a part of the  $2p - 2h$  channel because  $\Delta$  emission already includes  $2p - 2h$  decay inside the nucleus. Consequently, there is no unique way of separating the  $\Delta$  emission from the  $2p - 2h$  channels. In Refs. [15, 17], to separate  $2p - 2h$  channels, the imaginary part of the Delta propagator was subtracted and included into phenomenological inelastic contribution to the cross section. As a result, the MEC peak is located in the ‘‘dip’’ region between the QE and Delta peaks, i.e., the invariant mass of the pion-nucleon pair  $W^2 = (q + p_A)^2 = m^2 + 2m\omega - Q^2$  varies in the range  $(m_\pi + m) \leq W \leq 1.3 - 1.4$  GeV.

Each one of the four MEC operators can be decomposed as a sum of vector and axial-vector currents. In the axial part only the leading contribution to the axial-vector vertex proportional to the form-factor  $C_5^V$  is included. This form-factor is parametrized as [38]

$$G_A^5 = \frac{1.2}{(1 + Q^2/M_{A\Delta}^2)^2} \cdot \frac{1}{1 + Q^2/(3M_{A\Delta}^2)}, \quad (13)$$

with  $M_{A\Delta} = 1.05$  GeV.

In the present work we evaluate the electroweak MEC response functions  $R_{i,MEC}$  of lepton scattering on carbon, using accurate parametrizations of the exact MEC calculations [15, 17]. The functional forms employed for these parametrizations as functions of  $(\omega, |\mathbf{q}|)$  are valid in the range of momentum transfer  $|\mathbf{q}| = 200 \div 2000$  MeV. The expressions for the fitting parameters are described in detail in Refs. [16, 18, 39]. Results of lepton-nucleus cross sections obtained using these MEC parametrizations were successfully tested against the experimental world data for  $^{12}\text{C}$  [18, 28].

### III. RESULTS AND ANALYSIS

Before providing reliable predictions for neutrino scattering, any model must be validated by confronting it with quasielastic electron scattering data. To validate the RDWIA+MEC prescription we compare our results for the longitudinal and transverse responses, as well as for inclusive  $(e, e')$  cross sections, with experimental data. A consistent evaluation of these responses and cross sections is critical for a proper analysis of neutrino-nucleus interaction, as it allows to assess the validity of the RDWIA+MEC approach, at least in the vector sector.

#### A. Electromagnetic response functions and $^{12}\text{C}(e, e')$ cross sections

The longitudinal and transverse response functions on carbon calculated in the RDWIA+MEC approach are shown in Figures 1-3 for different values of the momentum transfer, together with Saclay [40] and the world data [41]. Note, that there are some differences between the two data sets because the world data exploited a wider range of the virtual photon polarization  $\epsilon = 0.05 \div 0.95$  for all  $|\mathbf{q}|$ -sets to reduce systematic errors in the Rothenbluth separation procedure. Also shows in figures are the contributions to  $R_L(|\mathbf{q}|, \omega)$  from the  $NN$ -correlated pairs and the contributions to  $R_T(|\mathbf{q}|, \omega)$  from the  $2p - 2h$  MEC. It is worth noting that, the influence of the short-range correlations on the transverse response is considerably smaller than on the longitudinal one, because the  $R_L$  is sensitive to the  $NN$ -correlations due to  $NN$ -interactions [42, 43].

The  $R_L(|\mathbf{q}|, \omega)$  and  $R_T(|\mathbf{q}|, \omega)$  responses as functions of energy transfer at  $|\mathbf{q}| = 300$

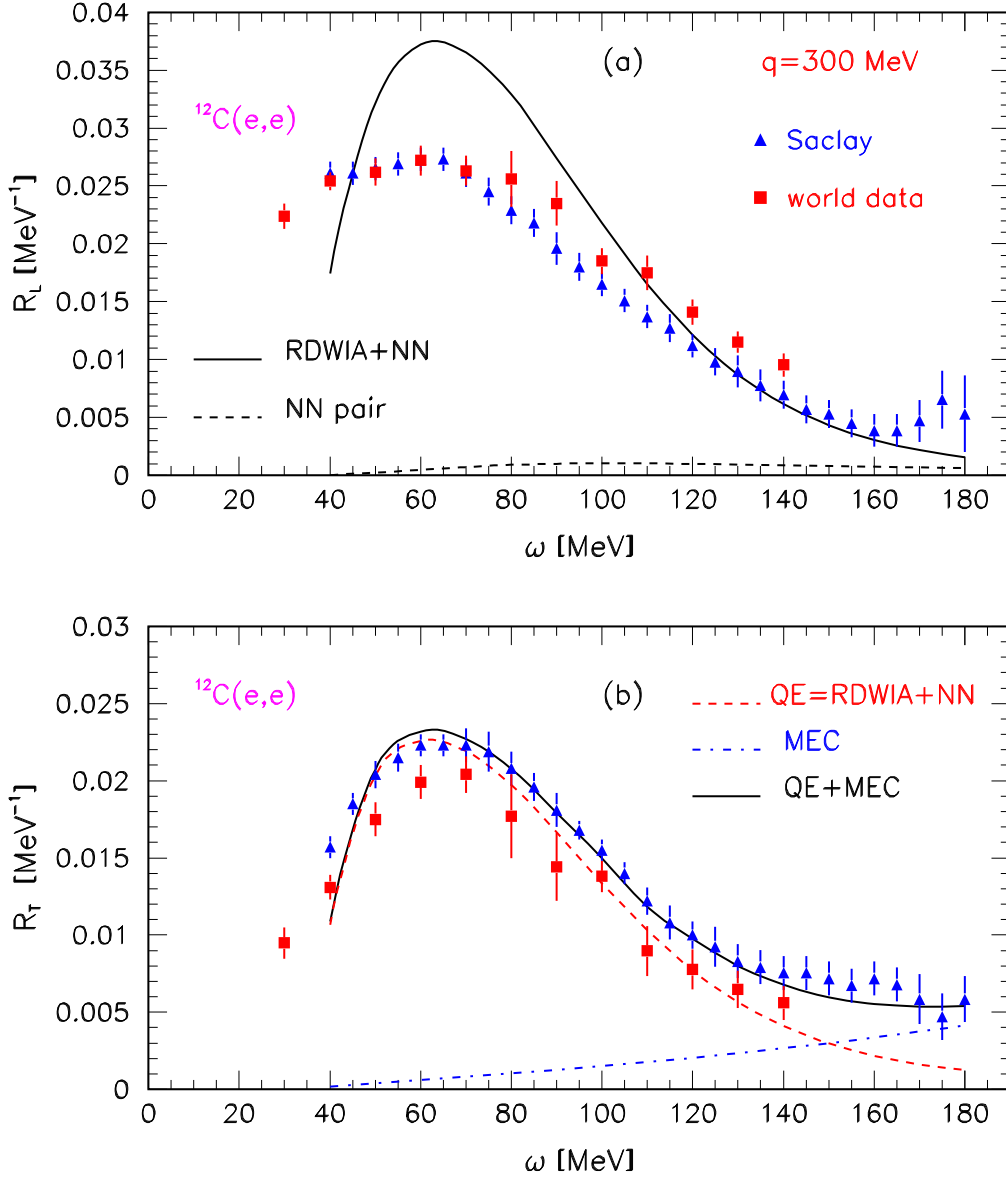


FIG. 1: (Color online) Longitudinal (a) and transverse (b) response functions at  $|\mathbf{q}| = 300 \text{ MeV}/c$  versus energy transfer  $\omega$  for electron scattering on  $^{12}\text{C}(e, e')$ . The solid line is the the RDWIA + MEC results, the dashed line is: the contribution from the  $NN$ -correlated pairs in (a) and the contribution from the RDWIA in (b). The dash-dotted line in (b) is the  $2p-2h$  MEC contributions. The data points are from Refs.[40, 41].

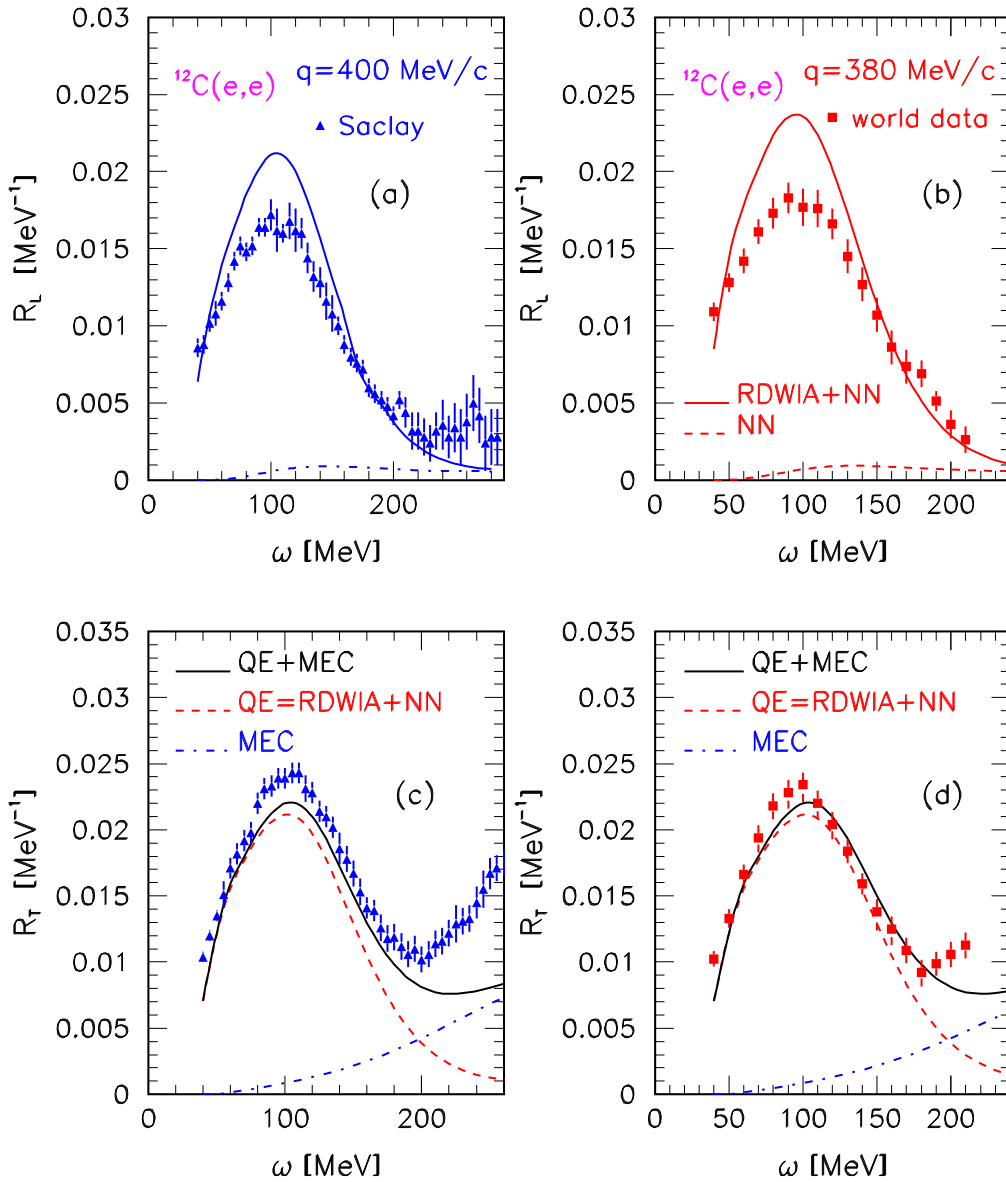


FIG. 2: (Color online) Same as in Fig. 1, but the longitudinal and transverse responses at  $|\mathbf{q}| = 400$  MeV/c are shown in (a), (c) and at  $|\mathbf{q}| = 380$  MeV/c in (b), (d). As shown in the key the data points are from Refs. [40, 41].

MeV/c are displayed in Fig. 1 with experimental results from Refs. [40, 41]. Apparently, the calculation overestimates the value of the  $R_L(|\mathbf{q}|, \omega)$  function, while the result for the  $R_T(|\mathbf{q}|, \omega)$  response is in good agreement with the data. The longitudinal and transverse responses for  $|\mathbf{q}| = 400, 380, 500, \text{ and } 570$  MeV/c are presented in Figs. 2, 3 and compared with data. The agreement between the RDWIA+MEC predictions and the world data is

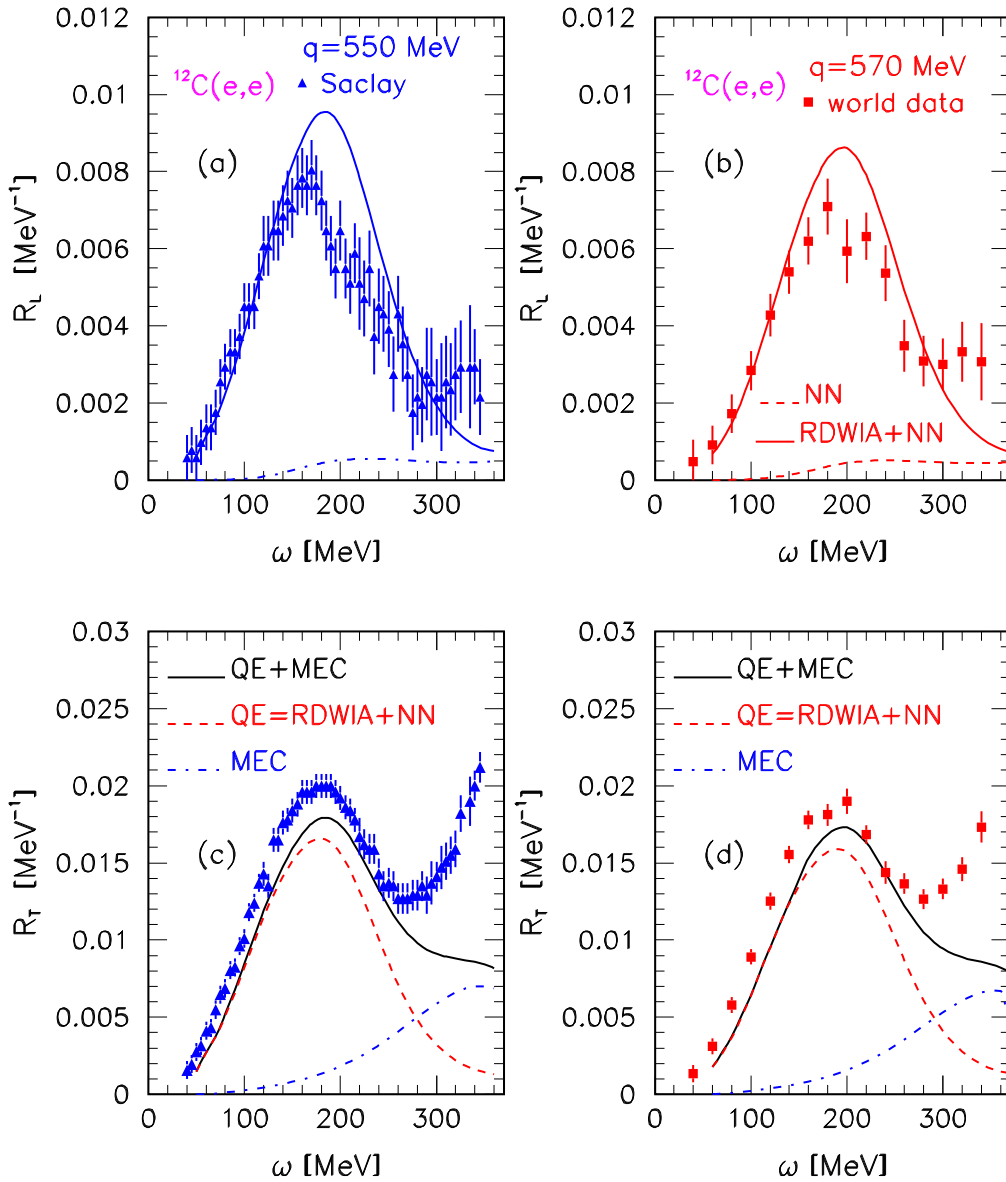


FIG. 3: (Color online) Same as in Fig. 2, but at  $|\mathbf{q}| = 550$  MeV/c and  $|\mathbf{q}| = 570$  MeV/c

quite satisfactory. It is obvious that the inclusion of the  $2p-2h$  MEC contributions increases the transverse responses at the high energy transfer and thereby improves the agreement with the data.

To test the RDWIA+MEC approach we calculated the double differential inclusive  $^{12}\text{C}(e, e')$  cross sections versus the energy transfer to the nucleus. Results are shown in Figs. 4, 5 and compared with the data from Ref. [40, 44–48]. In each panel we show the contributions to the inclusive cross section from QE and  $2p-2h$  MEC processes. The

comparisons were carried out for a wide range of kinematic variables, and each panel corresponds to fixed values of the incident electron energy and the scattering angle. The panels have been ordered according to the corresponding value for the momentum transfer at the quasi-elastic peak  $q_{QE}$ . There is a good agreement between cross sections calculated in the RDWIA+MEC approach and experimental data, thus validating the reliability of our predictions. The positions, widths, and heights of the QE peaks are reproduced by this model. Only at particular kinematics, i.e.  $E = 1500$  MeV,  $\theta = 11.95^\circ$ , and  $q_{QE} = 311$  MeV/c [44] the calculation overestimates the value of the cross section and the underestimation of the data at QE peak occurs at  $E = 500$  MeV,  $\theta = 60^\circ$ , and  $q_{QE} = 457$  MeV/c [45], while a good agreement is observed at close value  $q_{QE} = 443$  MeV/c, but at  $E = 730$  MeV and  $\theta = 37.1^\circ$  [46].

It should be pointed out that the contribution of the  $2p - 2h$  MEC increases with the energy transfer and reaches its maximum in the “dip” region between the QE and the  $\Delta$  peaks. In these calculations we do not consider the inelastic contributions that can have an effect on the  $(e, e')$  cross sections even in the QE regime. The inelastic part of the cross section is dominated by the delta peak (mainly transverse) that contributes to the transverse response function. In particular,  $\omega_{QE} = \sqrt{|\mathbf{q}|^2 + m^2} - m$  corresponds roughly to the center of the quasielastic peak,  $\omega_{\Delta} = \sqrt{|\mathbf{q}|^2 + m_{\Delta}^2} - m$  to the  $\Delta$ -resonance [ $m_{\Delta}$  is the mass of  $\Delta(1232)$ ], and region between the two peaks to the two-body excitations. When the momentum transfer is not too high these regions are clearly separated in data

$$\Delta\omega = \omega_{\Delta} - \omega_{QE} = \frac{(m_{\Delta}^2 - m^2)}{\sqrt{|\mathbf{q}|^2 + m^2} + \sqrt{|\mathbf{q}|^2 + m_{\Delta}^2}}, \quad (14)$$

allowing for a test of theoretical models for each specific process. At high momentum transfer the delta and QE peaks tend to overlap: in this case only the comparison with a complete model including inelastic processes is meaningful. In the present calculations only the real part of the Delta propagator is used and therefore the MEC peak is located in the range of  $W \approx 1.14 \div 1.16$  GeV. However, in the “frozen” MEC approximation [49] with the full Delta propagator, (with real and imaginary parts) the  $2p - 2h$  MEC peak position is located near the  $\Delta$  peak.

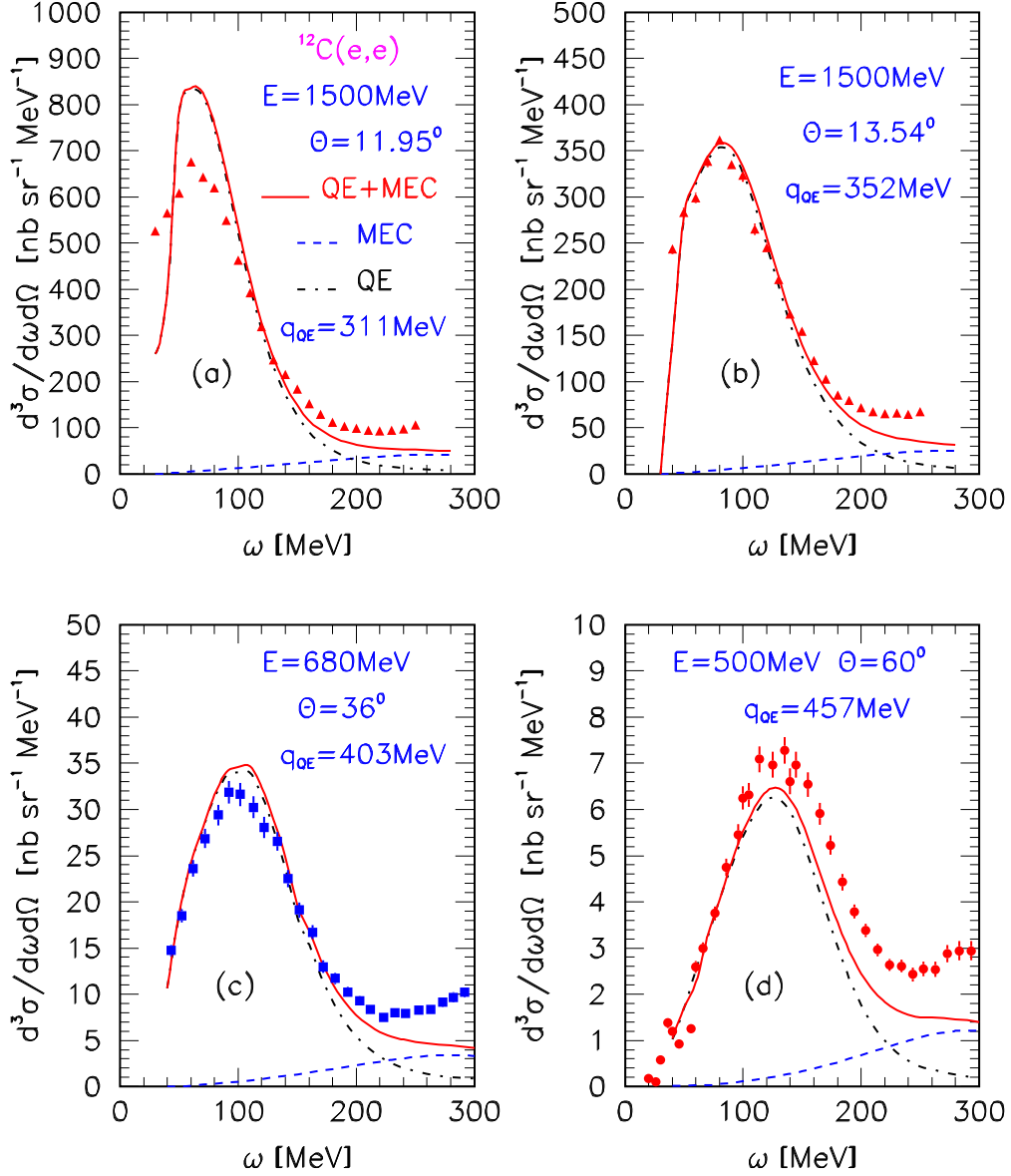


FIG. 4: (Color online) Inclusive cross section versus energy transfer  $\omega$  for electron scattering on  $^{12}\text{C}$ . The solid line is the RDWIA + MEC results, the dashed line is the  $2p-2h$  MEC contributions, and the dashed-dotted line is the contribution from the RDWIA. The data are from Ref. [44] (filled triangles), Ref. [40] (filled squares), Ref. [45] (filled circles). In Ref. [44] data are for the electron beam energy  $E = 1500$  MeV, and scattering angle  $\theta = 11.95^\circ, \theta = 13.54^\circ$ ; in Ref. [40] data are for  $E = 680$  MeV and  $\theta = 36^\circ$ ; in Ref. [45] data are for  $E = 500$  MeV and  $\theta = 60^\circ$ .

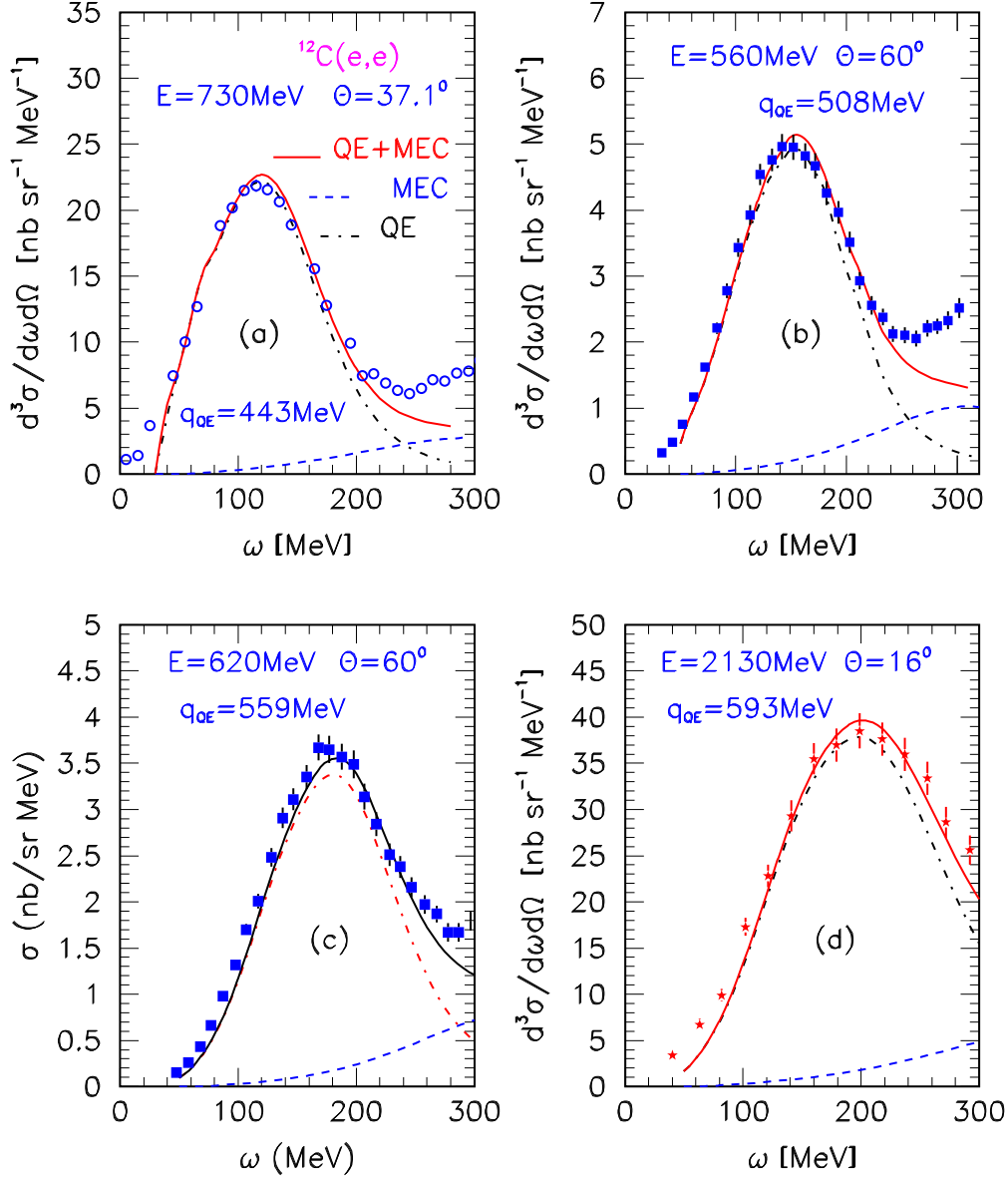


FIG. 5: (Color online) Same as in Fig. 4, but the data are from Ref. [46] (open circle) for the electron beam energy  $E = 730$  MeV and  $\theta = 37.1^\circ$ ; Ref. [40] (filled squares) for  $E = 560$  MeV and  $\theta = 60^\circ$  and  $E = 620$  MeV and  $\theta = 60^\circ$ ; Ref. [47, 48] for  $E = 2130$  MeV and  $\theta = 16^\circ$ .

## B. Neutrino cross sections

As was shown in Refs. [11–14, 18, 25, 50–52] two approaches can describe the enhanced cross sections observed in the MiniBooNE [51, 52] CCQE data: one which includes an enhanced transverse response due to the  $2p - 2h$  MEC [11–14, 18] with  $M_A \approx 1.03$  GeV,

and another is the impulse approximation approach [25, 50–52] with large value of  $M_A \approx 1.35$  GeV. For incoming neutrino energy  $\varepsilon_\nu = 2$  GeV we calculated neutrino and antineutrino cross sections  $(d\sigma/dx)_{QE+MEC}$  within the RDWIA+MEC model with  $M_A = 1.03$  GeV and  $(d\sigma/dx)_{M_A, QE}$  cross sections in the RDWIA approach with  $M_A = 1.35$  GeV as functions of  $x$ , where  $x = \varepsilon_\mu, Q^2, W$  are kinematic variables. To compare these distributions with the genuine CCQE  $(d\sigma/dx)_{QE}$  cross sections, obtained in the RDWIA model with  $M_A = 1.03$  GeV we also calculated  $R(MEC) = (d\sigma/dx)_{QE+MEC}/(d\sigma/dx)_{QE}$  and  $R(M_A = 1.35) = (d\sigma/dx)_{M_A, QE}/(d\sigma/dx)_{QE}$  ratios.

The inclusive  $d\sigma/d\varepsilon_\mu$  cross sections for neutrino and antineutrino scattering on carbon are presented in Fig. 6 as functions of muon energy. Here, on the upper panels the results obtained in the RDWIA+MEC approach are compared with  $(d\sigma/d\varepsilon_\mu)_{M_A, QE}$  inclusive cross sections. Also shown are the contributions of the  $2p - 2h$  MEC and genuine CCQE process to the  $(d\sigma/d\varepsilon_\mu)_{QE+MEC}$  cross section. The lower panels show the  $R(QE + MEC)$  and  $R(M_A = 1.35)$  ratios as functions of  $\varepsilon_\mu$ . One can observe that the  $2p - 2h$  MEC contribution increases with muon energy, reaching its maximum at  $\varepsilon_\mu \approx 1.6$  GeV, and becomes negligible in the region of the quasielastic peak. This leads to appearance of the peaks in the  $R(MEC)$  ratios in the energy range  $\varepsilon_\mu \approx 1.4 \div 1.7$  GeV. Both models predict an increase of cross sections relative to the  $(d\sigma/d\varepsilon)_{QE}$  results at low muon energies and show similar features near QE peak. Note that within the RDWIA model with  $M_A = 1.35$  GeV the cross sections in the region of the QE peak are predicted to be on  $\approx 10\%$  higher than  $(d\sigma/d\varepsilon)_{QE}$ .

Figure 7 shows the same as Fig. 6 but for  $d\sigma/dQ^2$  cross sections as functions of  $Q^2$ . At  $Q^2 < 0.2$  (GeV/c)<sup>2</sup> the RDWIA+MEC model results are about two times larger than  $(d\sigma/dQ^2)_{QE}$  cross sections. In the range  $0.2 < Q^2 < 1$  (GeV/c)<sup>2</sup> the ratio  $R(MEC) \approx 1.4$  and slowly decreases (increases) with  $Q^2$  for neutrino (antineutrino) scattering. Thus, in this  $Q^2$  range the  $2p - 2h$  MEC contribution changes slightly the slopes of the  $Q^2$ -distributions calculated within the RDWIA model with  $M_A = 1.03$  GeV/c<sup>2</sup>, because in the parametrization of the axial form factor  $G_A^5$  (13) the value of  $M_{A\Delta} \approx M_A \approx 1$  GeV is used. On the other hand, the  $R(M = 1.35)$  ratios increase with  $Q^2$  from  $R \approx 1$  at  $Q^2 \approx 0.1$  (GeV/c)<sup>2</sup> to 1.7 at  $Q^2 \approx 1$  (GeV/c)<sup>2</sup>.

Figure 8 shows the same as Fig. 6, but for  $d\sigma/dW$  cross sections as functions of  $W$ . The  $2p - 2h$  MEC contribution increases with invariant mass, and its maximum is located at  $W \approx 1.15$  GeV, as in the case of electron scattering. The ratio  $R(MEC)$  also increases with

$W$  from  $R \approx 1.1$  in the region of the QE peak up to 2.6(4.5) at  $W = 1.15$  GeV for neutrino (antineutrino) scattering. At  $W = 0.94$  GeV the ratio  $R(M_A = 1.35)$  is  $\approx 1.3$ , and it slowly increases up to  $\sim 1.6$  at  $W \approx 1.15$  GeV. Apparently, the MEC-effects dominate in the “dip” region.

The neutrino and antineutrino total cross sections  $\sigma_{tot}$  together with data [51–57] are presented in Fig. 9 as functions of the incoming neutrino energy. Here, the results obtained in the RDWIA+MEC approach are compared with the total cross sections calculated in the RDWIA model with  $M_A = 1.35$  GeV. Also shown are the RDWIA results with  $M_A = 1.03$  GeV, as well as contributions of the  $2p - 2h$  MEC that are about 27% at  $\varepsilon_\nu > 1$  GeV. The total cross sections are scaled with the number of neutron/proton in the target. From comparison of the RDWIA+MEC and RDWIA with  $M_A = 1.35$  GeV results it follows that the neutrino cross sections are in a good agreement and the difference between antineutrino cross sections is less than 10% at  $\varepsilon_\nu > 1$  GeV.

Thus, the analysis of the inclusive and total cross sections shows that the enhancement in either the transverse response, or in nucleon axial mass has almost the same effect on  $d\sigma/d\varepsilon_\mu$  and total cross sections, and they are different for  $Q^2$  and  $W$ -distributions.

However,  $Q^2$  and  $W$ -distributions are not functions of direct observables, because  $Q^2$  and  $W$  are inferred kinematic variables which depend on incoming neutrino energy that is not known in the neutrino experiments with their broad incoming neutrino energy distribution. Most notably, neutrino energy reconstruction is possible only in model-dependent ways. Therefore, there is a growing interest in measurements of the hadronic system kinematics which allows one to increase the accuracy of the calorimetric measurement of the incoming neutrino energy. All these developments will reduce our dependence on theoretical models.

#### IV. CONCLUSIONS

In this article, we studied quasielastic and  $2p - 2h$  MEC electron and (anti)neutrino scattering on a carbon target in the RDWIA+MEC and RDWIA with  $M_A = 1.35$  GeV approaches, placing particular emphasis on model dependence of the inclusive  $d\sigma/d\varepsilon_\mu$ ,  $d\sigma/dQ^2$ ,  $d\sigma/dW$ , and total cross sections.

In the RDWIA+MEC approach we calculated quasielastic contributions to lepton scattering cross sections, using the RDWIA model with  $M_A = 1.03$  GeV and MEC electroweak

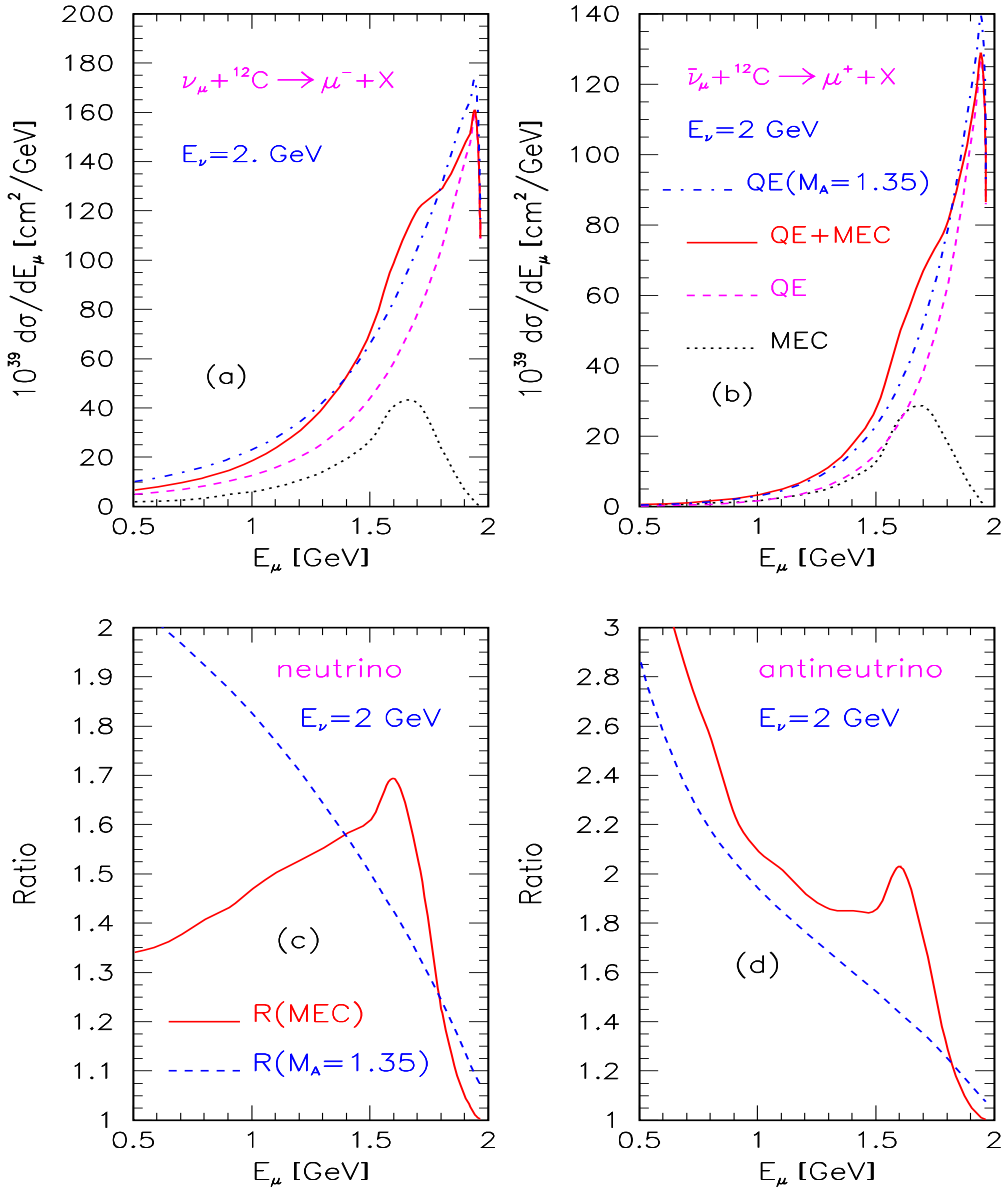


FIG. 6: (Color online) Inclusive cross section (upper panels) and ratios  $R(\text{MEC})$  and  $R(M_A = 1.35)$  (lower panels) vs the muon energy for neutrino and antineutrino scattering on  $^{12}\text{C}$  and for incoming neutrino energy  $\varepsilon_\nu = 2$  GeV. In the upper panels the solid line is the RDWIA+MEC calculation, the dash-dotted line is the RDWIA ( $M_A = 1.35$  GeV) calculation, whereas the dashed and dotted lines are the RDWIA( $M_A = 1.03$  GeV) and MEC contributions to the RDWIA+MEC cross sections. In the lower panel the solid and dashed lines are the  $R(\text{MEC})$  and  $R(M_A = 1.35)$  ratios, respectively.

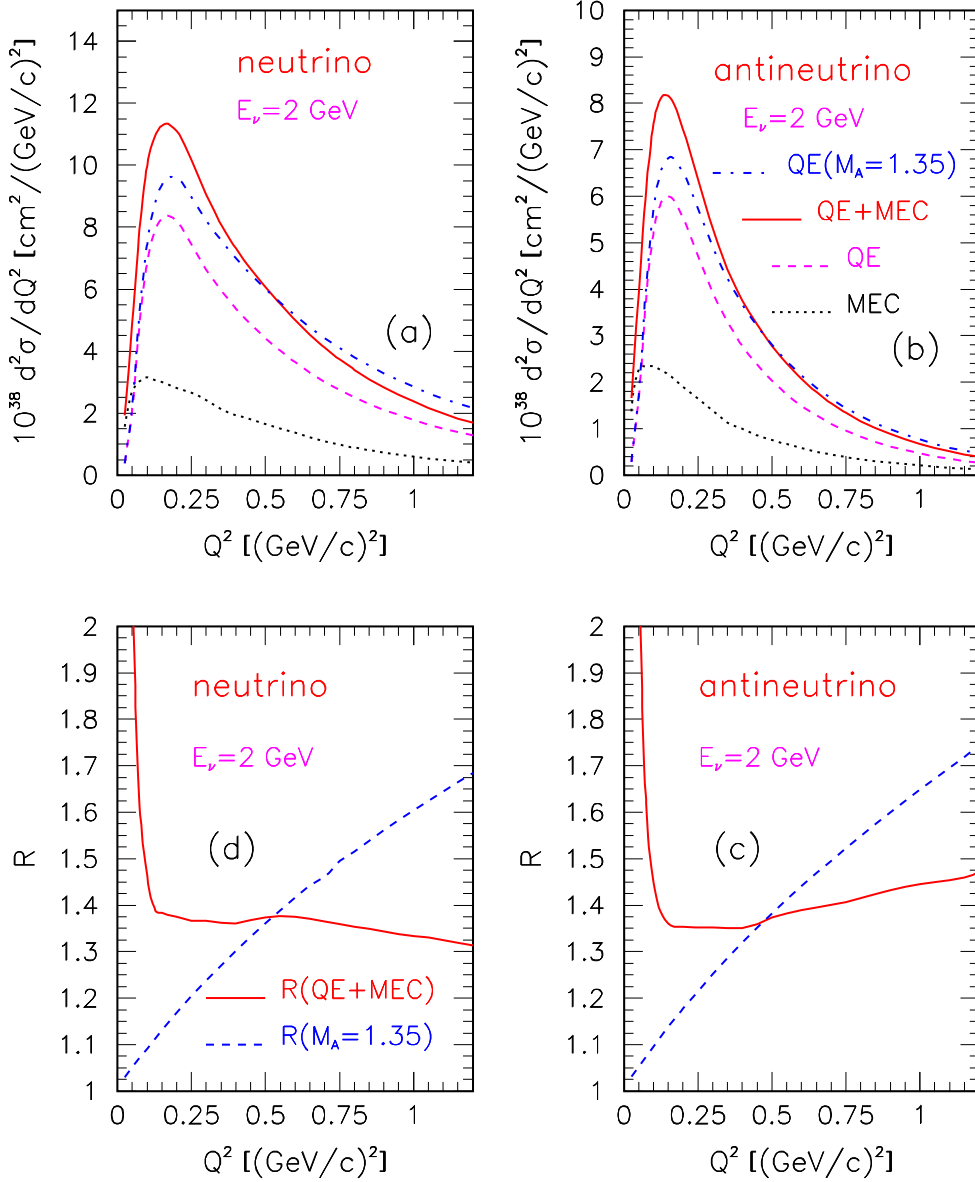


FIG. 7: (Color online) Same as in Fig. 6, but for  $d\sigma/dQ^2$  cross section vs the  $Q^2$ .

response functions obtained in the RFGM. In calculation of the inclusive and total cross sections within the RDWIA, the effects of FSI and short-range  $NN$ -correlations in the target ground state were taken into account. An accurate parametrization of the exact MEC calculations of the nuclear response functions was used to evaluate the MEC response. The RDWIA+MEC approach has been validated in the vector sector by describing the longitudinal and transverse response functions, as well as a set of inclusive electron scattering <sup>12</sup>C data.

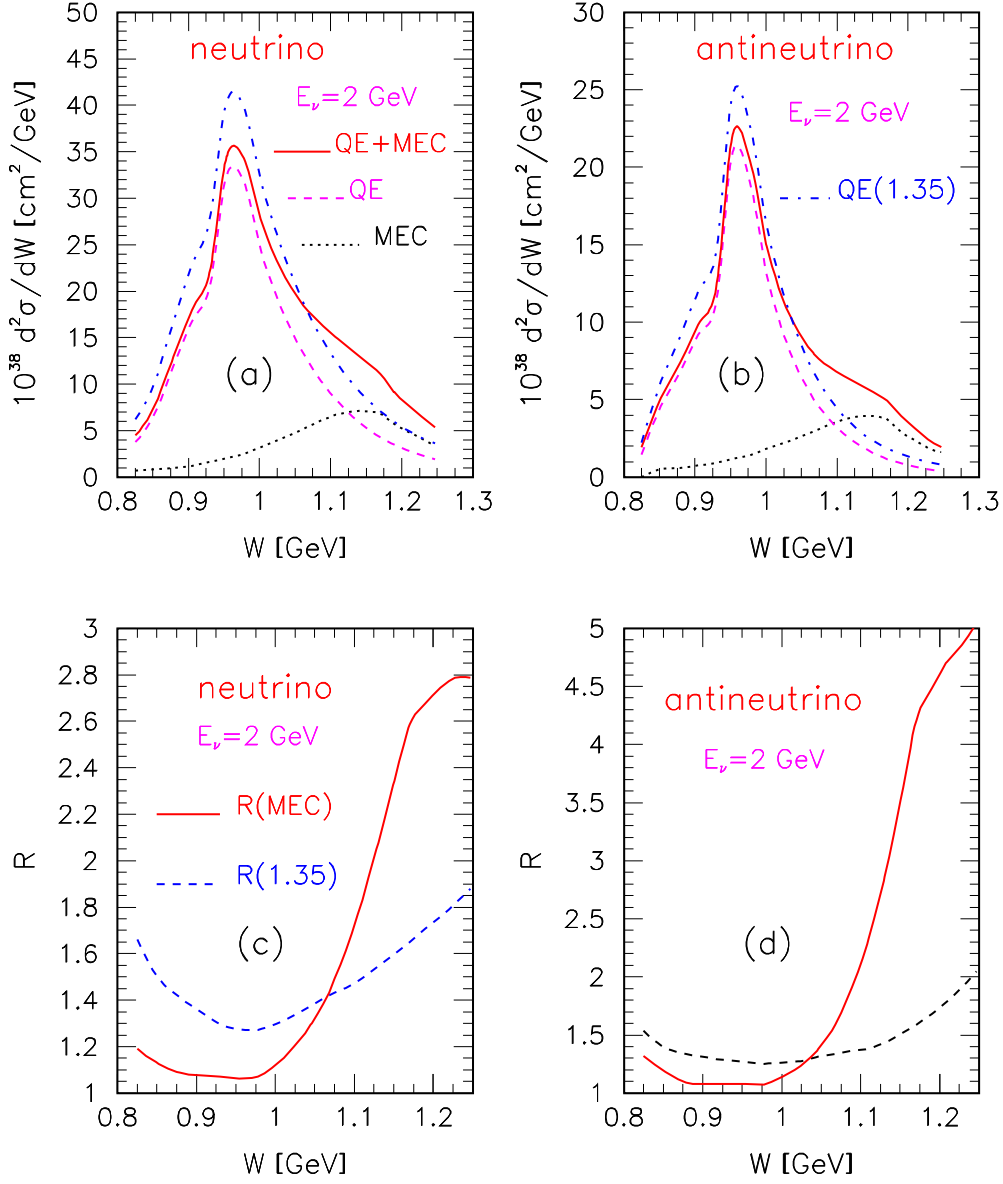


FIG. 8: (Color online) Same as in Fig. 6, but for  $d\sigma/dW$  cross section vs the  $W$ .

We compared the inclusive cross sections for neutrino energy  $\varepsilon_\nu = 2$  GeV and total (anti)neutrino cross sections obtained in these approaches and found that while the enhancement in the transverse response or in axial mass have almost the same effects on inclusive  $d\sigma/d\varepsilon_\mu$  and total cross sections this is not the case for the  $Q^2$  and  $W$ -distributions, where two effects can be distinguished. On the other hand,  $Q^2$  and  $W$  are inferred variables that depend on neutrino energy. Therefore, one needs the new experimental approaches that used hadronic information in order to increase the accuracy of the calorimetric method

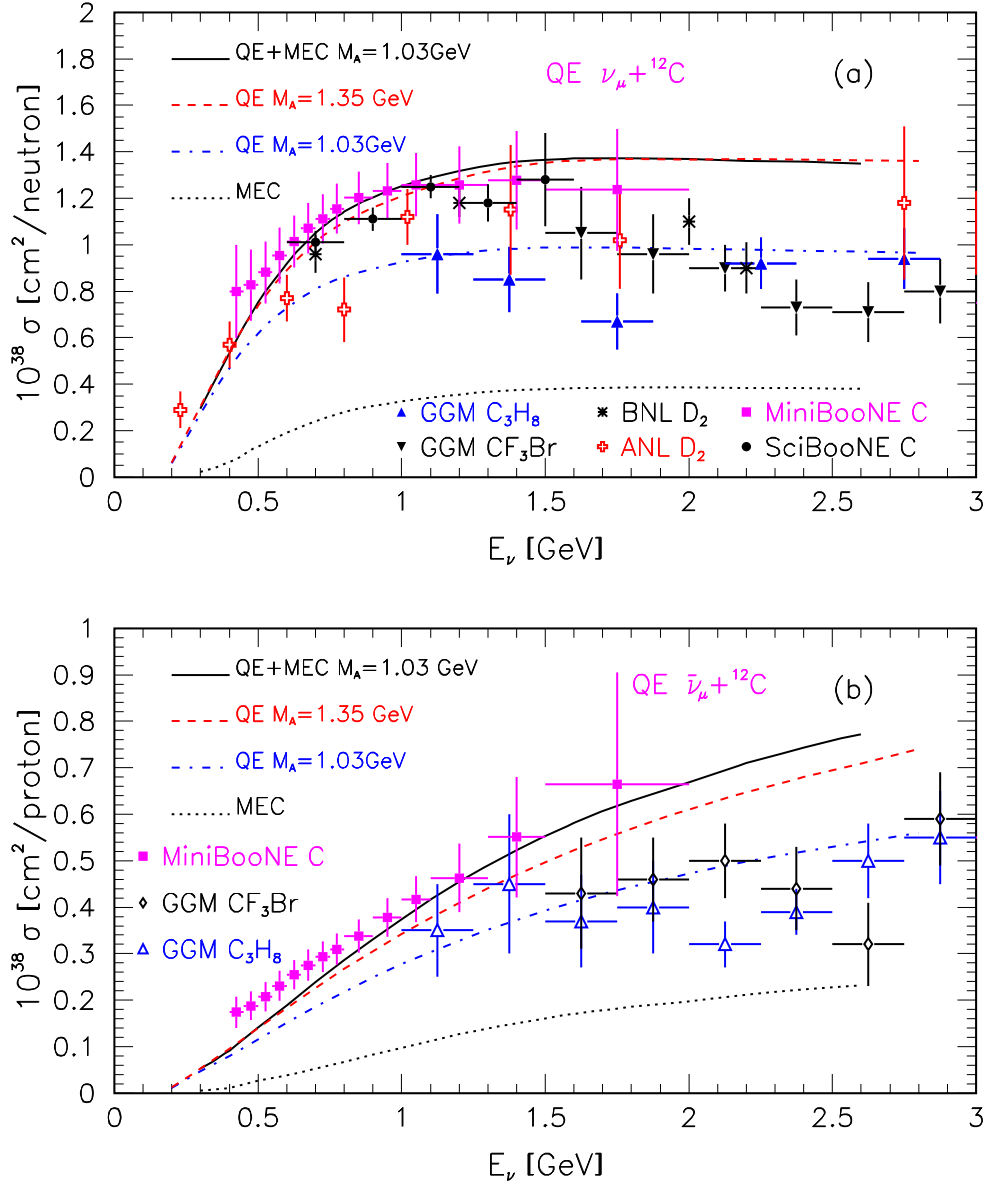


FIG. 9: (Color online) Total cross sections for QE and QE+MEC scattering of muon neutrino (upper panel) and antineutrino (lower panel) on  $^{12}\text{C}$  as a function of incoming (anti)neutrino energy. Data points for different targets are from Refs. [51–57]. Also shown are predictions of the RDWIA+MEC (solid line), RDWIA( $M_A = 1.35$  GeV) (dashed line), RDWIA( $M_A = 1.03$  GeV) (dash-dotted line), and  $2p - 2h$  MEC (dotted line).

of neutrino energy reconstruction in model-independent ways.

### Acknowledgments

The authors greatly acknowledge J. Amaro and G. Megias, for fruitful discussions and for putting in our disposal the codes for calculation of the MEC's electroweak response functions that were used in this work. We specially thank A. Lidvansky and J. Samoilova for a critical reading of the manuscript.

- 
- [1] NOvA Technical Design Report, FERMILAB-DESIGN-2007-01.
  - [2] P. A. Amaudrus *et al.*, (T2K Collaboration), Nucl. Instrum. Meth. **A686**, 1 (2012).
  - [3] R. Acciarri *et al.*, (DUNE Collaboration), FERMILAB-DESIGN-2016-03.
  - [4] Hyper-Kamiokande Design Report, KEK-PREPRINT-2016-21, ICRR-REPORT-701-2016-1.
  - [5] L. Wolfenstein, Phys. Rev. **D17**, 2369 (1978).
  - [6] S. P. Mikheyev and A.Y. Smirnov, Sov. J. Nucl. Phys. **42**, 913 (1985).
  - [7] P. Adamson *et al.*, (NOvA Collaboration), Phys. Rev. Lett. **118**, 151802 (2017).
  - [8] E. J. Moniz, Phys. Rev. **184**, 1154 (1969).
  - [9] G. T. Garvey, D. A. Harris, H. A. Tanaka, R. Tayloe, G. P. Zeller, Phys. Rept. **580**, 1 (2015).
  - [10] T. Katori, M. Martini, arXiv:1611.07770 [hep-ph].
  - [11] M. Martini, M. Ericson, and M. Chanfray, Phys. Rev. **C84**, 055502 (2011)
  - [12] M. Martini, and M. Ericson, Phys. Rev. **C87**, 065501 (2013).
  - [13] J. Nieves, I. Ruiz Simo, and M. J. Vicente Vacas, Phys. Lett. **B707**, 72 (2012).
  - [14] J. Nieves, I. Ruiz Simo, and M. J. Vicente Vacas, Phys. Lett. **B721**, 90 (2013).
  - [15] A. De Pace, M. Nardi, W. M. Alberico, T. W. Donnelly, and A. Molinari, Nucl. Phys. **A726**, 303 (2003).
  - [16] G. D. Megias, T. W. Donnelly, O. Moreno, C. F. Williamson, J. A. Caballero, R. Conzalez-Jimenez, A. De Pace, M. Barbaro, W. M. Alberico, M. Nardi, and J. E. Amaro, Phys. Rev. **D91**, 073004 (2015).
  - [17] I. Ruiz Simo, J. E. Amaro, M. B. Barbaro, A. De Pace, J. A. Caballero, and T. W. Donnelly, J. Phys. **G44**, 065105 (2017).

- [18] G. D. Megies, J. E. Amaro, M. B. Barbaro, J. A. Caballero, T. W. Donnelly, and I. Ruiz Simo, Phys. Rev.**D94**, 093004 (2016).
- [19] J. J. Kelly, Adv. Nucl. Phys. **23**, 75 (1996).
- [20] K. G. Fissum *et al.*, Phys. Rev. **C70**, 034606, 2004
- [21] J. J. Kelly, Phys. Rev. **C71**, 064610 (2005).
- [22] C. Maieron, M. C. Martinez, J. A. Caballero, and J. M. Udias, Phys. Rev. **C68**, 048501 (2003).
- [23] A. Meucci, C. Giusti, and F. D. Pacati, Nucl. Phys. **A739**, 277 (2004).
- [24] A. V. Butkevich and S. A. Kulagin, Phys. Rev. **C76**, 045502 (2007).
- [25] A. V. Butkevich, Phys. Rev. **C82**, 055501 (2010).
- [26] A. V. Butkevich, and D. Perevalov, Phys. Rev. **C84**, 015501 (2011).
- [27] A. V. Butkevich, Phys. Rev. **C85**, 065501 (2012).
- [28] G. D. Megies, J. E. Amaro, M. B. Barbaro, J. A. Caballero, T. W. Donnelly, Phys. Rev.**D94**, 013012 (2016).
- [29] T. de Forest, Nucl. Phys. **A392**, 232 (1983).
- [30] P. Mergell, U.-G. Meissner, and D. Drechsel, Nucl. Phys. **A596**, 367 (1996).
- [31] B. Serot, J. Walecka, Adv. Nucl. Phys. **16**, 1 (1986).
- [32] C. J. Horowitz D. P. Murdock, and Brian D. Serot, in *Computational Nuclear Physics 1: Nuclear Structure* edited by K. Langanke, J. A. Maruhn, Steven E. Koonin (Springer-Verlag,Berlin, 1991), p.129.
- [33] D. Dutta *et al.*, Phys. Rev. **C68**, 064603 (2003).
- [34] D. Rohe *et al.*, Nucl. Phys. B (Proc. Suppl.) **159**, 152 (2006).
- [35] J. J Kelly, <http://www.physics.umd.edu/enp/jjkelly/LEA>
- [36] E .D. Cooper, S. Hama, B. C. Clark, and R. L. Mercer, Phys. Rev. **C47**, 297 (1993).
- [37] Ciofi degli Atti and S. Simula, Phys. Rev. **C53** , 1689 (1996).
- [38] E. Hernandez, J. Nieves, and M. Valverde, Phys. Rev. **D76** , 033005 (2007).
- [39] G. D. Megias and J. E. Amaro, Private communication.
- [40] P. Barreau *et al.*, Nucl. Phys. **A402** 515, (1983).
- [41] J. Jourdan, Nucl. Phys.**A603**, 117 (1993).
- [42] R. Schiavilla, A. Fabrocini, and V. R. Pandharipande, Nucl. Phys. **A473**, 290 (1987).
- [43] J. Carlson, R. Schiavilla, Rev. Mod. Phys. **70**, 743 (1998).
- [44] D. Baran *et al.*, Phys. Rev. Lett. **61**, 400 (1988).

- [45] R. R. Whitney, I. Sick, J. R. Ficenec, R. D. Kephart, and W. P. Trower, *Phys. Rev.* **C9**, 2230 (1974).
- [46] J. S. O'Connell *et al.*, *Phys. Rev.* **C35** 1063,
- [47] O. Benhar, D. Day, and I. Sick, *Rev. Mod. Phys.* **80** 189 (2006).
- [48] O. Benhar, D. Day, and I. Sick, *Rev. Mod. Phys.* arXiv:nucl-ex/0603032 (2006).
- [49] I. Ruiz Simo, J. E. Amaro, M. B. Barbaro, J. A. Caballero, G. D. Megias, and T. W. Donnelly, arXiv:1611.07770 [hep-ph].
- [50] A. V. Butkevich, and D. Perevalov, *Phys. Rev.* **D89** 053014, (2014).
- [51] A. A. Aguilar-Arevalo *et al.*, (MiniBooNE Collaboration), *Phys. Rev.* **D81**, 092005 (2010).
- [52] A. A. Aguilar-Arevalo *et al.*, (MiniBooNE Collaboration), *Phys. Rev.* **D88**, 032001 (2013).
- [53] J. L. Alcaraz-Aunion and J. Walding (SciBooNE Collaboration), *AIP Conf. Proc.* **1189**, 145 (2009).
- [54] W. A. Mann *et al.*, *Phys. Rev. Lett.* **31**, 844 (1973).
- [55] N. J. Baker *et al.*, *Phys. Rev.* **D23**, 2499 (1981).
- [56] M. Pohl *et al.*, *Lett. Nuovo Cim.* **26**, 332 1979.
- [57] J. Brunner *et al.*, *Z. Phys.* **C45**, 551 1990.